Research Article Vol. 8, No. 8 / August 2021 / Optica 1113

optica

Enhancing high-order harmonic generation by controlling the diffusion of the electron wave packet

T. Severt,[1,†] J. Troß,[1,†] G. Kolliopoulos,[1] I. Ben-Itzhak,[1,3] and C. A. Trallero-Herrero[1,2,4]

[1]J. R. Macdonald Laboratory, Department of Physics, Kansas State University, Manhattan, Kansas 66506, USA
[2]Department of Physics, University of Connecticut, Storrs, Connecticut 06269, USA
[3]e-mail: ibi@phys.ksu.edu
[4]e-mail: carlos.trallero@uconn.edu

Received 16 February 2021; revised 17 May 2021; accepted 29 June 2021 (Doc. ID 422711); published 17 August 2021

We experimentally study the enhancement of high-order harmonic generation (HHG) driven by synthesized $\omega - 3\omega$ laser fields, where we control whether the ionization rate or the electron wave packet's diffusion is the dominant enhancement mechanism. When minimizing the electron wave packet's diffusion, the excursion times of the corresponding electron trajectories are reduced by a factor of 2 or more. This result is important for imaging techniques that use the returning electron wave packet to probe the remaining ion. Furthermore, we achieve a 10× to 3800× enhancement of the harmonic yield driven by the bichromatic fields relative to that of an optimized single-color field, showing that the bichromatic fields improve HHG's capability as a light source. We also measure that the two-color field's harmonics have half the divergence angle compared to their single-color counterpart, suggesting that the "short" electron trajectories play a more prominent role compared to their "long" trajectory counterparts, thus improving the wavefront of the emerging harmonic beam.

https://doi.org/10.1364/OPTICA.422711

1. INTRODUCTION

Following the strong-field ionization of atoms or molecules, the intense oscillatory electric field of a laser may accelerate the ejected photoelectron back toward the remaining parent ion [1–3]. During the recollision, this photoelectron may, for example, recombine with the parent ion and emit radiation in a process known as high-order harmonic generation (HHG) [4–6] or rescatter off the parent ion, creating a structured high-energy photoelectron spectrum [7,8]. In each of these cases, the returning electron wave packet can be used as a probe to study the structure and dynamics of the target immediately following ionization and is the underlying idea of high-harmonic spectroscopy (HHS) [9–19] and laser-induced electron diffraction (LIED) [20–25].

One challenge in using the rescattering electron wave packet as a probe is that the classical excursion times associated with each trajectory determine when the remaining ion is probed. To tune the excursion times, researchers try to control the returning trajectories by manipulating the ionizing electric fields. For example, Blaga *et al.* [21] controlled the electron trajectories' excursion times by changing their laser's wavelength to probe O_2 and N_2 molecules via LIED. Alternatively, Brugnera *et al.* [26] proposed controlling and enhancing the so-called "long" electron trajectory contributions in HHG using orthogonally polarized $\omega - 2\omega$ laser fields, allowing them to probe the remaining ion at different times compared to the "short" trajectories. While both of these examples accomplish the goal of probing the remaining parent ion at different times, it is beneficial to develop alternative methods that take advantage of the dominant short-trajectory electrons and are relatively simple to implement.

In this paper, we experimentally demonstrate a method that significantly changes the excursion time of the short-trajectory electrons by controlling the relative phase and intensities of a bichromatic $\omega - 3\omega$ laser field. Even though our proof-of-principle measurement is demonstrated using HHG from argon, our results should be applicable to any electron rescattering-based process, since it has been shown that the Coulomb potential of the remaining ion has little effect on the electron trajectories [2,25,27].

In addition to HHG's importance as a spectroscopic tool for imaging the structure and dynamics of the target molecule, it also has shown promise as a table-top source of coherent extreme ultraviolet (XUV) to soft x-ray radiation with attosecond pulse durations [6]. Since its discovery, researchers have investigated various methods to increase the photon flux produced by HHG and improve the beam quality to make it a more viable light source [6,28–38].

One approach to enhance the photon flux of HHG-based laser sources is to build driving lasers that produce higher pulse energies and repetition rates to generate harmonics [6,28–30]. An alternative approach is to increase HHG's conversion efficiency, which is typically on the order of 10^{-5} or lower [2,3]. Many techniques focus on the macroscopic conversion efficiency through improving the phase matching of HHG [2,3,39,40], either by controlling the plasma defocusing mechanism in the medium [31] or by changing

the geometry of the target medium using gas cells [32–34] or gas-filled waveguides [35–38]. Other approaches focus on enhancing the single-atom or molecule conversion efficiency by changing the wavelength of the driving fields [15,41–45] or using multicolor fields [46–62].

Focusing on multicolor driving fields, Jin *et al.* [58] theoretically proposed using $\omega - 3\omega$ laser fields to enhance the HHG yield by 2 orders of magnitude. Since macroscopic phase matching favors short trajectory electrons, their idea is that bichromatic fields can be tuned to enhance HHG by boosting the ionization rates leading to a subset of electron trajectories that return to the remaining ion and maximize the contributions of the short trajectory electrons compared to other competing trajectories.

In this paper, we study the phase-dependent enhancement of HHG driven by two-color 800-266-nm laser fields over their optimized single-color counterparts. When performing this measurement, we chose to fix the input pulse energy, since this situation represents the real-world scenario where the output power of the driving laser is limited. In this case, we observe a 10× to 3800× enhancement over the 800-nm field, which is optimized for maximum high-harmonic photon flux by adjusting its pulse energy and focusing conditions.

Furthermore, we relate the relative two-color phase optimizing each harmonic order above the ionization threshold of the target gas to its corresponding electron trajectories by simultaneously measuring the ionization in the target medium. By tuning the relative intensities between the fields, we demonstrate control over whether the quantum diffusion, i.e., dispersion, of the electron wave packet or the ionization rate plays a larger role in maximizing the resulting high-order harmonic yield. To our knowledge, this is the first experimental evidence of such control.

Finally, the smaller divergence angle of the enhanced harmonics produced by the two-color fields compared to the 800-nm field supports the assertion that we are optimizing the short over the long trajectories, since they can be distinguished in the far field [26,63,64]. More importantly, by optimizing the short trajectories, we improve the wavefront of the resulting photon beam, allowing for better refocusing of the emerging harmonic beam after its generation [64], thus increasing the potential applicability of HHG-based light sources driven by $\omega - 3\omega$ laser fields.

2. EXPERIMENTAL SETUP

This section briefly describes our experimental setup, shown schematically in Fig. 1(a). We specifically focus on the unique aspects of our setup compared to other standard HHG setups, e.g., see Refs. [60–62] and previous iterations of our own setup described elsewhere [65,66]. A more complete description of the experimental setup can be found in Supplement 1.

We produce the 800-266-nm driving laser fields using a two-color interferometer, where the third harmonic is generated in a single arm, labeled arm B in Fig. 1(a), using a standard setup of BBOs, calcite, and wave plates [42,67]. There are several unique features of our interferometer worth noting. First, we tune the dispersion of the 800-nm pulse propagating through arm A, shown in Fig. 1(a), to simultaneously maximize the harmonic yield, cutoff photon energy, and ionization rate in the target gas, creating the shortest pulse possible on target. In other words, we tune the dispersion of that pulse by adjusting the compressor grating to compensate for transmission through the wave plate, beam splitters, air, and entrance window into the vacuum chamber. On the other hand, the 800-nm pulse that traverses arm B has negative dispersion, since it does not travel the same optical path. Therefore, to compensate for this negative dispersion and maximize the third-harmonic generation, we insert a 2-mm thick SF11 glass plate before the third harmonic generation (THG) setup located in arm B. This way, we minimize the dispersion experienced by each optical path while simultaneously maximizing the third-harmonic conversion efficiency. Second, to stabilize the interferometer, we dampen vibrations by isolating the breadboard it is built on from the optical table using mechanical vibration isolation mounts (Newport VIB100). Without any external optical feedback, we measured an RMSE stability of about 50 as over 3 min by imaging the interference pattern of a CW laser. The time-dependent interference pattern is shown in Fig. 1(b) and the resulting phase stability in Fig. 1(c). Given that the optical period of the 266-nm laser field is approximately 900 as, this high stability enables a two-color phase-control measurement.

We then use the bichromatic field to generate harmonics in a thin argon gas jet, introduced into the vacuum chamber via a glass capillary with an inner diameter of 250 μm, i.e., approximately a factor of 5 less than the Raleigh range of the focused 266-nm laser beam. We use a thin target to minimize volume averaging and propagation effects that would complicate the results' interpretation. In Supplement 1, we include additional details about the beam widths in the gas jet, the position of the gas jet with respect to the focus of the driving fields, and how we spatially overlap the beams within the generation medium. Finally, we image the generated harmonics using a standard flat-field spectrometer [68]. To determine the optimal conditions for the single- and two-color driving fields, we adjust the focus of the laser with respect to the gas jet to maximize the yield of the plateau harmonics. A sample of raw harmonics spectra, i.e., before applying any efficiency corrections or background subtraction, are included in Supplement 1.

Perhaps most importantly, we simultaneously measure the ionization yield caused by the driving field's interaction with the argon target using a channeltron detector located approximately 2.5 cm from the jet. Specifically, the voltage on the channeltron detector is set to attract the argon ions, with an approximate electric-field strength of 20 V/mm in the interaction region.

3. RESULTS

This section presents our experimental findings for HHG enhancement by 800–266 nm laser fields over its single-color counterparts. Specifically, we explore the enhancement for two different intensity ratios, one where the intensity of each color is approximately equal with values of 1.3×10^{14} and 1.0×10^{14} W/cm^2, respectively, which we refer to as (1.3:1.0) throughout the rest of the paper. The second is an unequal intensity ratio of (3.0:0.4), i.e., a third-harmonic intensity of about 10% the fundamental. We observe 1 to 3 orders of magnitude of HHG enhancement driven by the two-color fields compared to the single-color 800-nm field.

Furthermore, we exhibit control over whether the ionization rate or electron wave packet's diffusion is the dominant enhancement mechanism by changing the relative intensity ratios between the two colors. To our knowledge, this is the first experimental demonstration of such control. Finally, the divergence angle of the harmonic beams produced by the two-color fields is generally half

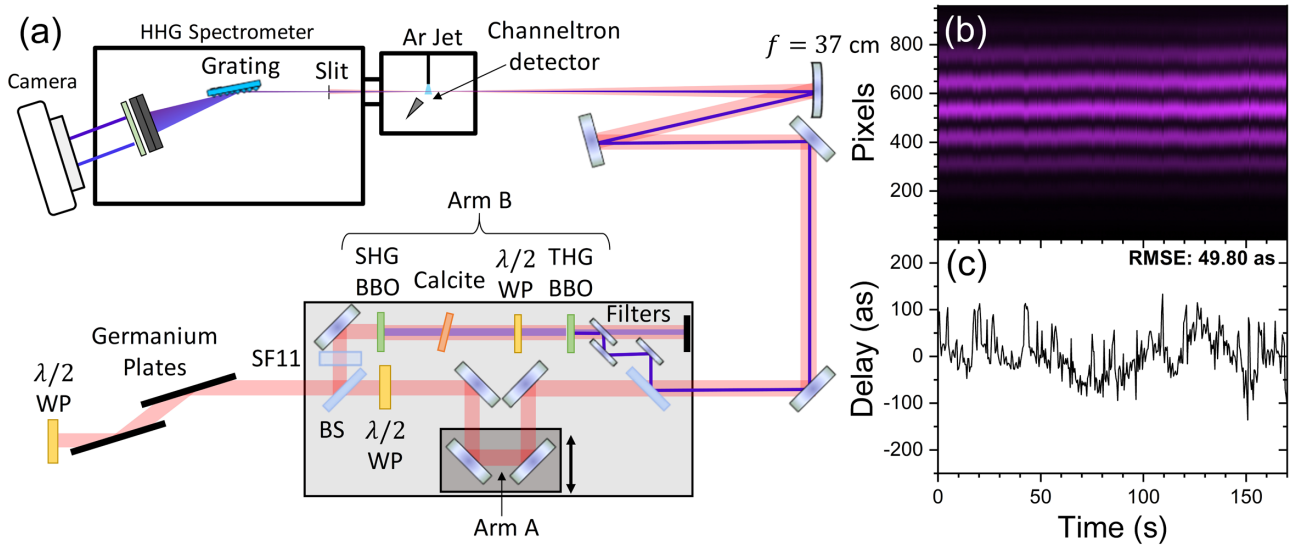

Fig. 1. (a) Schematic of the experimental setup (see text and Supplement 1 for description). (b) Measured interference pattern of a continuous-wave laser at the output of the interferometer, which is used to determine the stability of the interferometer. (c) Fourier analysis of (b) demonstrating a vibrational stability of 49.8 as over 170 s without any external feedback to the interferometer. Note that all axes in panels (b) and (c) are plotted using linear scales.

of the single-color 800-nm driving field, suggesting that the short trajectories are enhanced compared to the long trajectories.

A. HHG Enhancement

For experimentalists, the main limiting factor for increasing the high-harmonic photon flux is the maximum energy per pulse their laser provides, assuming a fixed repetition rate. Therefore, when comparing harmonics produced from the different driving fields, we use the same pulse energies before the interferometer as the single-color 800-nm driving field's pulse energy. Likewise, for the single-color 266-nm field, we fix the pulse energy at the input of the optics generating the third harmonic. Then, to maximize the overall harmonic yield, we adjust the focusing conditions. It is worth noting that the two-color and single-color fields driving HHG do not have the same pulse energy due to the third harmonic's conversion efficiency, which is about 15% of the 800-nm pulse's energy input into the third-harmonic generation's mixing crystals. Nevertheless, we observe significant enhancements in the harmonic yields despite the lower total pulse energy on target of the two-color driving fields. For more information about the input pulse energies, see Supplement 1.

In Fig. 2(a), we plot the harmonics yields for the optimized single color 800- and 266-nm fields as well as for both two-color intensity ratios. These yields are integrated over the divergence angle and bandwidth as well as corrected for each harmonic's detection efficiency (see Supplement 1). For the two-color fields, it is worth noting that the relative phase between the fields is chosen to independently maximize each individual harmonic's yield. Furthermore, Fig. 2(b) shows the enhancement for both intensity ratios of the bichromatic driving fields and single-color 266-nm field with respect to the single-color 800-nm field. Specifically, we define the enhancement as the integrated photon yield produced by the two-color or 266-nm field divided by the yield of our optimized 800-nm field. We observe that both intensity ratios outperform the optimized 800-nm field by at least 1 order of magnitude.

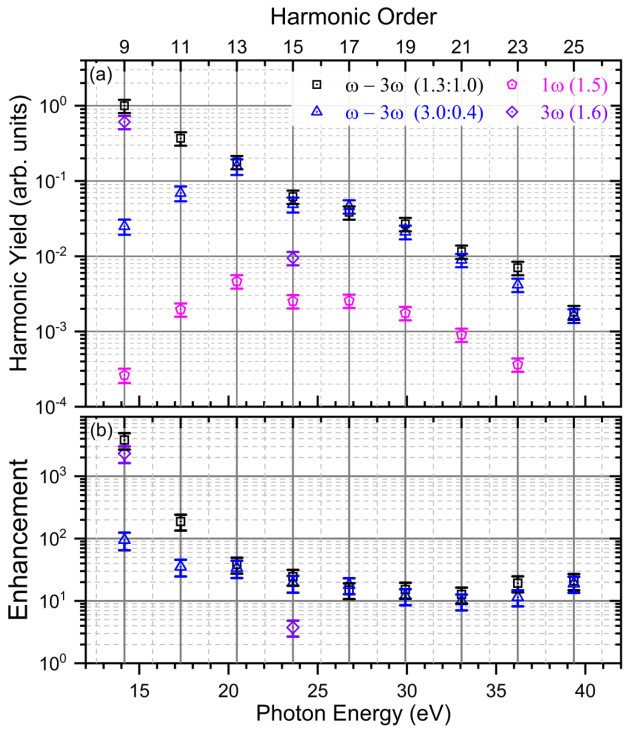

Fig. 2. (a) Harmonic yields driven by ω (pink), 3ω (purple), and $\omega - 3\omega$ for the (3.0:0.4) (blue) and (1.3:1.0) (black) intensity ratios; (b) Enhancement of harmonics generated by the 800-266-nm fields over the optimized single-color 800-nm. All graphs are shown as a function of photon energy and harmonic order (top axis). Note that the x axes of these plots are scaled linearly while the y axes are scaled logarithmically.

For photon energies above 20 eV, both two-color intensity ratios approximately enhance the HHG photon yield by about 1 order of magnitude. The main difference between these ratios is observed in the resulting beam's divergence angles, which is further described in Subsection 3.C. For photon energies below 20 eV, the approximately equal (1.3:1.0) intensity ratio leads to larger enhancement. Specifically, the 9th and 11th harmonics

outperform the single-color driving field by 3 and 2 orders of magnitude, respectively. It is important to note that the photon energy of the 9th harmonic lies below the ionization threshold of argon at 15.76 eV [69], while the 11th harmonic is located slightly above. It has been shown that resonances can play a prominent role in the generation of below- and near-threshold harmonics (see the review by Xiong *et. al.* [70]). In the case of argon, the ninth harmonic at 14.2 eV lies near several Rydberg states, such as the $3s^2\,3p^5(^1P^o_{1/2})^3D$ [69], which may help significantly enhance the harmonic's yield. To determine the roles of these resonances, calculations and more careful experiments must be conducted in the future. For our experiment, the difference in enhancement between the two intensity ratios is mainly attributed to the significantly stronger third-harmonic field, which dominates the production of the ninth harmonic, as shown for the optimized 266-nm driving field.

B. Phase-Dependent HHG Yield

To determine the electron trajectories that optimize each harmonic's yield, we perform a two-color phase-dependent measurement of the HHG and ionization yields simultaneously. Specifically, in Fig. 3(a), we show the harmonic yield, integrated over the divergence angles, as a function of the relative phase (time delay) between the colors of the bichromatic 800-266-nm laser field and the photon energy for the approximately equal (1.3:1.0) intensity ratio. Figure 3(c) shows a similar plot, but for the unequal intensity ratio of (3.0:0.4). It is worth noting that in Figs. 3(a) and 3(c), we normalize the maximum yield of each harmonic to unity to help visualize the phase dependence. Additionally, the magenta symbols in Figs. 3(a) and 3(c) denote when each harmonic is maximized within one period of the oscillations. We also show the associated normalized integrated ion yield for the (1.3:1.0) and (3.0:0.4) intensity ratios in Fig. 3(b). Specifically, we scaled both ionization yields such that the maximum value of the (1.3:1.0) ratio is normalized to unity, demonstrating that the ionization yield is 5.4 times higher for the (3.0:0.4) intensity ratio. For the rest of this section, we focus on interpreting the observed phase shift between the ionization and the maximum yield of each harmonic.

The phase-dependent total ionization yield provides us with an *in situ* measurement of the relative phase between the laser fields because the yield is expected to peak when the two-color fields are in phase [71]. Therefore, since we know the pulses are not significantly chirped from our frequency resolved optical gating (FROG) measurements, we can determine the combined electric field that is expected to contribute most to our observed signals, i.e., near the peak intensity of the Gaussian envelope of the pulse. With this information, we then unambiguously relate the measured phase corresponding to the maximum harmonic yield to its associated electron trajectories. As we demonstrate in this section, the phase shifts between the maximum harmonic yield and ionization rate suggest that the observed enhancement is not simply due to the increased intensity of the bichromatic field, as the harmonics are not maximized when $\phi_q - \phi_i = 0$.

To determine the relative phase shift between each harmonic order and the peak ionization yield, we fit the function

$$Y_{q,i}(t) = A_{q,i}\cos\left(3\omega t + \phi_{q,i}\right) + y_{q,i} \tag{1}$$

to the ionization yield and integrated yield of each harmonic. In the above equation, the subscripts q and i refer to the q^{th} harmonic and the ionization, respectively, ω is the frequency of the fundamental field, $\phi_{q,i}$ is the phase shift, $A_{q,i}$ is the amplitude of the oscillation, and $y_{q,i}$ is the yield offset from 0. At this point, it is worth noting that we arbitrarily set the time delay (relative phase) axes in Figs. 3(a)–3(c) such that the extracted ϕ_i is zero. In Fig. 3(d), we show the extracted phase shifts ϕ_q of each harmonic with respect to the ionization, i.e., $\phi_q - \phi_i$, for both intensity ratios. It is worth mentioning that the line traced by the magenta points in Figs. 3(a) and 3(c) appears "flipped" compared to the one shown in Fig. 3(d) due to the time to frequency conversion.

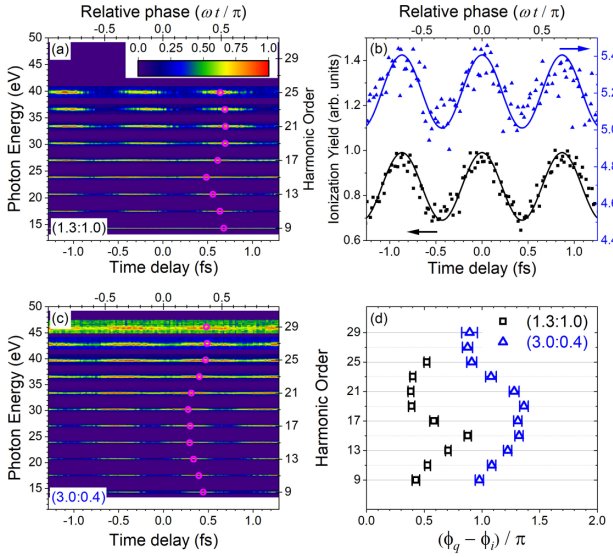

Fig. 3. (a) Measured harmonic yield integrated over divergence angles as a function of the time delay (i.e., relative phase) and the photon energy of the two-color 800-266-nm field for the intensity ratio of (1.3:1.0). Note that the maximum amplitude for each harmonic is scaled to unity to help visualize the phase-dependent yield oscillations. The magenta symbols denote the phases at which each harmonic is maximized, as extracted from the fits (see text). (b) The scaled ionization yields as a function of the time delay between the fields for the (1.3:1.0) and (3.0:0.4) intensity ratios, denoted by the black and blue symbols, respectively, are associated with the y axis of the same color. The solid lines display the fits to the data. The data for both intensity ratios are scaled such that the maximum value of the (1.3:1.0) intensity ratio is unity, demonstrating that ionization is a factor of 5.4 higher for the (3.0:0.4) ratio. (c) Same as panel (a), except for an intensity ratio of (3.0:0.4); (d) extracted phase shifts for each harmonic order (ϕ_q) with respect to the peak ionization yield (ϕ_i) for both intensity ratios; the displayed uncertainty is at the 2σ level. Note that all axes in this figure are scaled linearly.

To interpret the observed phase shifts, we must first understand what physical mechanisms affect the HHG yield at the macroscopic and single-atom level. Macroscopically, we employ a thin gas jet (nozzle diameter of 250 μm) to minimize phase-mismatching effects along the propagation direction of the laser, such as modification of the driving field due to absorption and dispersion as well as the reabsorption of the generated high harmonics [2,3,38–40,72,73]. As shown in Refs. [74,75], ionization provides a natural method for quantitative determination of phase-matching conditions as it is an *in situ* measurement of the number of emitters. While not shown here, we routinely check phase-matching conditions through the ionization yield and harmonic cutoff. Our conditions are very similar to that of Shiner *et. al.* [74], where they measured the wavelength scaling of HHG's efficiency at the single-atom level. Therefore, interpreting the phase shift

between the maximum ionization and harmonic yields at the single-atom level should be a reasonable approximation under our experimental conditions.

At the single-atom level, HHG can be explained using the three-step model [27,76,77], where an electron is ionized, accelerated in the laser field, and then recombined with the parent ion emitting a photon. Furthermore, from the quantum mechanical strong-field approximation (SFA), i.e., the Lewenstein model [27], we know that the main mechanisms influencing the harmonic yield are the ionization rate and the electron wave packet's dispersion while traversing the continuum, which appears like a classical excursion time within the expression for the time-dependent dipole (see Supplement 1 for further discussion). It is worth noting that within this model, the recombination probability is independent of the electric field as long as the ionization of the medium is small enough to not deplete the ground state. Furthermore, it is important to note that the classical electron trajectories are approximately equivalent to the trajectories predicted using SFA (Lewenstein model) within the saddle-point approximation [3,27]. Therefore, our simulations referred to throughout the rest of the paper show the classical trajectories, which are calculated using the standard approach for two-color fields [2] and are explained further in Supplement 1. We also only focus on the short trajectory electrons because the diffusion of the wave packet and the macroscopic phase matching favors them over the long trajectories, especially when the focus is located before the target gas jet [2,39], as is the case in our experiment. It is important to note that the explanations given above (in this paragraph) are only applicable to the harmonics with photon energies above the ionization potential of the argon target. Therefore, in this section, we only focus on the phase dependence of those harmonics.

Figures 4(a) and 4(b) show the excursion times of the possible trajectories returning within one cycle of the fundamental field leading to the central photon energies of the 15th and 19th harmonics, as a function of the relative phase between the two-color laser fields for the intensity ratio of (1.3:1.0). The measured phase $\phi_q - \phi_i$ that optimizes each harmonic is marked by the solid black vertical lines, and the line colors correspond to the electric field strength normalized to its maximum possible value when the two-color fields are in phase. Interestingly, each harmonic exhibits complicated phase-dependent structure in the short trajectories, i.e., trajectories with excursion times shorter than 1.5 fs. For example, the 15th harmonic trajectory's excursion times, shown in Fig. 4(a), change by about a factor of 2. Specifically, we find that the excursion time changes from 0.54 fs at $\phi = 0.5\pi$ to 1.15 fs at 1.3π. Notably, the measured harmonic yield is maximized when the trajectory's excursion time is approximately shortest instead of when the electric field strength, and hence the ionization, is largest. This result suggests that the wave packet's diffusion has the largest influence on enhancing each harmonic's yield. It is important to note that in the region where the excursion time is shortest, i.e., from about $0 - \pi$ for the 15th harmonic, the experimentally measured phase optimizing the harmonic yield shifts to the right side of the region where the electric field strength is stronger. In other words, the phase corresponds to a "Goldilocks zone" where the combination of the relatively large ionization rate and the smaller quantum diffusion lead to the maximum harmonic yield. We observe similar behavior for the other harmonics, but show only the 15th and 19th harmonics for brevity.

For the unequal (3.0:0.4) intensity ratio in Fig. 4(c), we show the corresponding phase-dependent trajectories as previously

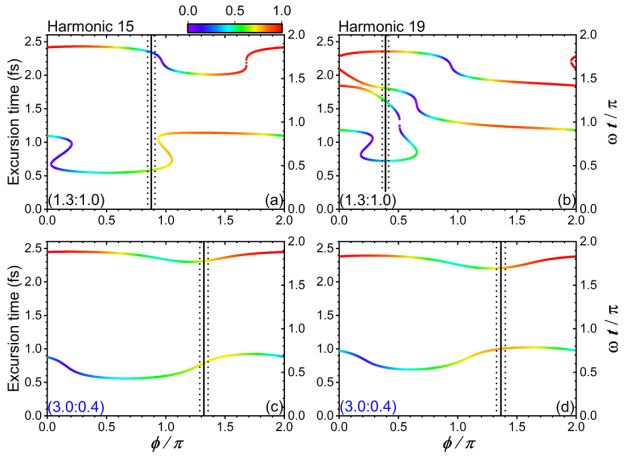

Fig. 4. Excursion times of the classical electron trajectories contributing to the (a) 15th and (b) 19th harmonics, as a function of relative phase between the 800- and 266-nm laser fields for the approximately equal intensity ratio of (1.3:1.0). The colors of the lines represent the normalized strength of the electric field at the time of ionization for each trajectory. The solid black vertical lines show the measured phase corresponding to the maximum harmonic yields, while the dotted lines represent the uncertainty (at the 2σ level). Similarly, panels (c) and (d) show the equivalent plots but for an intensity ratio of (3.0:0.4). Note that all axes in this figure are scaled linearly.

explained for the 15th harmonic. It is important to note that the other harmonics follow similar trends, where we show harmonic 19 as an example in Fig. 4(d). Surprisingly, this intensity ratio exhibits a strikingly different behavior compared to the equal intensity ratio. For example, the short trajectories' excursion times do not change as much, only changing from about 0.56 fs at $\phi = 0.75\pi$ to about 0.92 fs at 1.7π for the 15th harmonic. Also, the maximized harmonic yield picks out the phases near where the ionization rate for that trajectory is maximized, though slightly shifted towards shorter excursion times.

Our experimental results demonstrate that tuning the intensity ratio of the bichromatic driving field allows one to control whether the ionization rate when the wave packet is launched or the wave packet's diffusion while traversing the continuum has a larger influence over enhancing the harmonic yield. Furthermore, by tuning the relative phase between the fields with an intensity ratio of (1.3:1.0), we control the dispersion of the wave packet on attosecond time scales, changing the excursion times of the electrons by a factor of 2 or more. This significant control over the electron's excursion times is applicable to various methods that rely on the timing of the rescattering electron wave packet to probe the system's dynamics.

Finally, and perhaps most importantly, this control over the rescattering electron wave packet is expected to be independent of the fundamental wavelength of the driving $\omega - 3\omega$ laser field. Therefore, by going to fundamental fields with longer central wavelengths, the change in excursion times can be further increased, providing researchers with a broader range of recollision times to probe the remaining ion.

It is worth noting that our phase-dependent results suggest a means to increase the resulting harmonics' yield by finding intensity ratios that maximize the ionization rates at phases for which the excursion time of the short electron trajectories is the shortest. Hopefully, by exploring this further and combining it with other enhancement techniques that exploit different phase-matching

mechanisms, like using gas cells [32–34] or waveguides [35–38], the larger enhancements theoretically predicted by Jin *et. al* [58] may be reached.

C. HHG Divergence

Studying HHG's divergence is important in measuring the harmonic beam's wavefront quality. Since the accumulated dipole phase for the short and long trajectories have different intensity dependencies [78–80], each trajectory's contribution is maximized for different phase-matching conditions [2,64]. Focusing on the harmonic's divergence, the spatial intensity profile of the laser leads to the long and short trajectories separating spatially in the far field, where the long trajectories typically have a larger divergence angle than the short trajectories [26,63,64]. This separation in the far field gives rise to chromatic aberrations [64,81,82] that affect the spatial quality and wavefront of the refocused harmonic beam. Therefore, to minimize the aberrations, it is beneficial to minimize the contributions of the long trajectories both on the macroscopic and single-atom level. In our experiment, we placed the focus of all driving fields before the target gas jet, thus minimizing the contributions of the long trajectories [2,39]. Furthermore, theoretical work by Jin *et al.* [58] suggests that two-color driving fields may further decrease the contributions of the long trajectories. To explore whether this is the case, we compare the divergence of the bichromatic fields to the single-color 800-nm field.

In Fig. 5, we show the measured divergence of the harmonics generated by the bichromatic and single-color driving fields. In particular, Fig. 5(a) shows the measured harmonic spectrum as a function of the photon energy and divergence angle for the 800-266-nm driving fields for the (1.3:1.0) intensity ratio. Note that the relative phase between the two-color field chosen is the average of the phases shown in Fig. 3(d) for this intensity ratio. It is important to note that each harmonic's maximum value in Fig. 5(a) is scaled to unity to help visualize the divergence better. In Fig. 5(b), we compare the yields of the 17th harmonic as a function divergence angle for both two-color intensity ratios as well as the single-color 800-nm driver. From this plot, it is clear that the bichromatic fields significantly outperform the 800-nm driving field.

To quantitatively compare the divergence of each harmonic order, in Fig. 5(c) we plot the measured full-width divergence angle at $1/e^2$ of the maximum intensity as a function of harmonic order for the bichromatic and single-color driving fields. For the harmonics produced by the two-color fields, we plot the divergence angle at the phase where each harmonic's flux is maximized. One can see that, for most harmonic orders, the bichromatic fields produce less divergent beams than the 800-nm field. This result is consistent with the assertion by Jin *et al.* [58] that HHG by $\omega - 3\omega$ driving fields enhances the short over the long trajectories. Furthermore, the (1.3:1.0) intensity ratio produces smaller divergence harmonics than the (3.0:0.4) ratio, with the exception of the ninth harmonic. This result may arise from the difference in excursion times of the electron trajectories for each intensity ratio, though this calls for further investigation. It is important to note that the ninth harmonic may have a significantly different divergence angle due to contributions of resonances [70] in argon [69], as discussed in Subsection 3.A.

It is worth noting that there are two other conditions of our experiment that also may assist in minimizing the divergence of the generated harmonics. First, since we are generating the third harmonic in one arm of the interferometer instead of before the interferometer, we eliminated the wavefront distortions in the 800-nm beam due to depletion during the third-harmonic generation process. Second, as discussed in Supplement 1, the beam diameter of the third harmonic is about 75% the size of the diameter of the fundamental beam. As a result, we are spatially selecting the central portion of the fundamental driving field, which may also assist in minimizing the divergence of the harmonics by decreasing the contributions generated further off-axis.

To reiterate the important message of this subsection, the bichromatic fields produce harmonic beams with smaller divergences due to minimizing the contributions of the long trajectories. Since the short and long trajectories have different wavefronts and phases, minimizing the long trajectories allows the resulting beams to have better wavefronts, improving the focusing quality and brightness of the photon source.

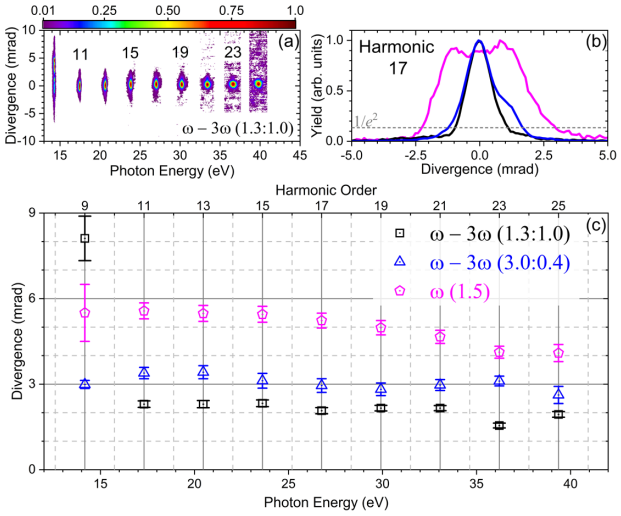

Fig. 5. (a) Photon yield as a function of the photon energy and divergence angle for the intensity ratios (1.3:1.0); several harmonic orders are marked on the figure for clarity; (b) integrated yield of the 17th harmonic as a function of its divergence angle for the single- and two-color laser fields, normalized so the maximum value is set to unity; the color coding follows the legend in panel (c); (c) measured full-width divergence angle at $1/e^2$ of the maximum intensity of each harmonic order for the single- and two-color driving fields. Note that all axes in these plots are scaled linearly.

4. CONCLUSION AND OUTLOOK

We explored the phase-dependent enhancement of HHG driven by $\omega - 3\omega$ laser fields for two different intensity ratios, namely, when the intensities are approximately equal (1.3:1.0) and significantly different (3.0:0.4). By measuring the phase-dependent harmonic spectrum and ionization yields simultaneously, each harmonic's phase dependence is related to its corresponding electron trajectories. Then, one can control whether the ionization rate or the electron wave packet's diffusion plays the dominant role in enhancing HHG by tuning the intensity ratios and relative phase between the two colors. Furthermore, for the (1.3:1.0) intensity ratio, the recolliding electron's classical excursion time is changed by a factor of 2 or more. Finally, we show that the enhancement and divergence of HHG driven by the bichromatic fields compared to the 800-nm field produce brighter harmonics (by 1 to 3 orders of magnitude) and less divergent beams (by a factor of 2).

Our results are applicable to a wide variety of situations in strong-field-induced rescattering physics. While the HHG's enhancement may be unique to our specific experimental conditions, the significant change in the electron's classical excursion times as a function of relative phase is independent of the driving-field's wavelengths. Therefore, we expect similar results for a variety of bichromatic driving fields, as long as the intensity ratio is properly selected. In addition, the relative-phase-dependent change in the electron's excursion time has the potential to control when the returning electron wave packet probes the remaining ion, which is crucial in HHS and LIED techniques.

One may improve upon our results by exploring other phase-matching media, such as gas cells and waveguides, or by finding the optimal intensity ratios that simultaneously maximize the ionization rates and minimize excursion times of the short trajectories. Also, the improved divergence of the harmonic beams produced by the $\omega - 3\omega$ fields indicates that the long electron trajectory contributions are significantly suppressed, therefore improving the beam's spatial and temporal qualities, which can be beneficial for spectroscopy, coherent imaging, and industrial metrology applications [64].

Funding. U.S. Department of Energy (DE-FG02-86ER13491, DE-SC0019098); National Science Foundation (1229672, IIA-1430493); U.S. Department of Defense (A2386-12-1-3014).

Acknowledgment. We would like to acknowledge Cheng Jin and C. D. Lin for inspiring us to pursue this research. Furthermore, we would like to thank Bincheng Wang and C. D. Lin for useful discussions about the strong-field approximation model for HHG. We would also like to thank K. D. Carnes for assistance with the final manuscript. T. S. was partially supported by the NSF. C. A. T.-H. was partially funded by U.S. Department of Energy.

Disclosures. The authors declare no conflicts of interest.

Data availability. Data underlying the results presented in this paper are not publicly available at this time but may be obtained from the authors upon reasonable request.

Supplemental document. See Supplement 1 for supporting content.

[†]These authors contributed equally to this paper.

REFERENCES

1. C. J. Joachain, N. J. Kylstra, and R. M. Potvliege, *Atoms in Intense Laser Fields* (Cambridge University, 2009).
2. Z. Chang, *Fundamentals of Attosecond Optics* (CRC Press, 2011).
3. C. D. Lin, A.-T. Le, C. Jin, and H. Wei, *Attosecond and Strong-Field Physics* (Cambridge University, 2018).
4. K. Midorikawa, "High-order harmonic generation and attosecond science," Jpn. J. Appl. Phys. **50**, 090001 (2011).
5. V. V. Strelkov, V. T. Platonenko, A. F. Sterzhantov, and M. Y. Ryabikin, "Attosecond electromagnetic pulses: generation, measurement, and application. generation of high-order harmonics of an intense laser field for attosecond pulse production," Phys. Usp. **59**, 425 (2016).
6. C. M. Heyl, C. L. Arnold, A. Couairon, and A. L'Huillier, "Introduction to macroscopic power scaling principles for high-order harmonic generation," J. Phys. B **50**, 013001 (2017).
7. D. D. Hickstein, P. Ranitovic, S. Witte, X.-M. Tong, Y. Huismans, P. Arpin, X. Zhou, K. E. Keister, C. W. Hogle, B. Zhang, C. Ding, P. Johnsson, N. Toshima, M. J. J. Vrakking, M. M. Murnane, and H. C. Kapteyn, "Direct visualization of laser-driven electron multiple scattering and tunneling distance in strong-field ionization," Phys. Rev. Lett. **109**, 073004 (2012).
8. W. Becker, S. P. Goreslavski, D. B. Milošević, and G. G. Paulus, "The plateau in above-threshold ionization: the keystone of rescattering physics," J. Phys. B **51**, 162002 (2018).
9. J. Itatani, J. Levesque, D. Zeidler, H. Niikura, H. Pépin, J. C. Kieffer, P. B. Corkum, and D. M. Villeneuve, "Tomographic imaging of molecular orbitals," Nature **432**, 867–871 (2004).
10. S. Baker, J. S. Robinson, C. A. Haworth, H. Teng, R. A. Smith, C. C. Chirilâ, M. Lein, J. W. G. Tisch, and J. P. Marangos, "Probing proton dynamics in molecules on an attosecond time scale," Science **312**, 424–427 (2006).
11. B. K. McFarland, J. P. Farrell, P. H. Bucksbaum, and M. Guhr, "High harmonic generation from multiple orbitals in N_2," Science **322**, 1232–1235 (2008).
12. D. Shafir, Y. Mairesse, D. M. Villeneuve, P. B. Corkum, and N. Dudovich, "Atomic wavefunctions probed through strong-field light–matter interaction," Nat. Phys. **5**, 412–416 (2009).
13. O. Smirnova, Y. Mairesse, S. Patchkovskii, N. Dudovich, D. Villeneuve, P. Corkum, and M. Y. Ivanov, "High harmonic interferometry of multielectron dynamics in molecules," Nature **460**, 972–977 (2009).
14. H. J. Wörner, J. B. Bertrand, D. V. Kartashov, P. B. Corkum, and D. M. Villeneuve, "Following a chemical reaction using high-harmonic interferometry," Nature **466**, 604–607 (2010).
15. A. D. Shiner, B. E. Schmidt, C. Trallero-Herrero, H. J. Worner, S. Patchkovskii, P. B. Corkum, J.-C. Kieffer, F. Legare, and D. M. Villeneuve, "Probing collective multi-electron dynamics in xenon with high-harmonic spectroscopy," Nat. Phys. **7**, 464–467 (2011).
16. P. M. Kraus, B. Mignolet, D. Baykusheva, A. Rupenyan, L. Horný, E. F. Penka, G. Grassi, O. I. Tolstikhin, J. Schneider, F. Jensen, L. B. Madsen, A. D. Bandrauk, F. Remacle, and H. J. Wörner, "Measurement and laser control of attosecond charge migration in ionized iodoacetylene," Science **350**, 790–795 (2015).
17. M. Lein, "Molecular imaging using recolliding electrons," J. Phys. B **40**, R135 (2007).
18. S. Haessler, J. Caillat, and P. Salières, "Self-probing of molecules with high harmonic generation," J. Phys. B **44**, 203001 (2011).
19. J. P. Marangos, "Development of high harmonic generation spectroscopy of organic molecules and biomolecules," J. Phys. B **49**, 132001 (2016).
20. M. Meckel, D. Comtois, D. Zeidler, A. Staudte, D. Pavicic, H. C. Bandulet, H. Pepin, J. C. Kieffer, R. Dörner, D. M. Villeneuve, and P. B. Corkum, "Laser-induced electron tunneling and diffraction," Science **320**, 1478–1482 (2008).
21. C. I. Blaga, J. Xu, A. D. DiChiara, E. Sistrunk, K. Zhang, P. Agostini, T. A. Miller, L. F. DiMauro, and C. D. Lin, "Imaging ultrafast molecular dynamics with laser-induced electron diffraction," Nature **483**, 194–197 (2012).
22. B. Wolter, M. G. Pullen, A.-T. Le, M. Baudisch, K. Doblhoff-Dier, A. Senftleben, M. Hemmer, C. D. Schröter, J. Ullrich, T. Pfeifer, R. Moshammer, S. Gräfe, O. Vendrell, C. D. Lin, and J. Biegert, "Ultrafast electron diffraction imaging of bond breaking in di-ionized acetylene," Science **354**, 308–312 (2016).
23. K. Amini, M. Sclafani, T. Steinle, A.-T. Le, A. Sanchez, C. Müller, J. Steinmetzer, L. Yue, J. R. M. Saavedra, M. Hemmer, M. Lewenstein, R. Moshammer, T. Pfeifer, M. G. Pullen, J. Ullrich, B. Wolter, R. Moszynski, F. J. G. de Abajo, C. D. Lin, S. Gräfe, and J. Biegert, "Imaging the Renner–Teller effect using laser-induced electron diffraction," Proc. Natl. Acad. Sci. USA **116**, 8173–8177 (2019).
24. F. Brausse, F. Bach, F. Krečinić, M. J. Vrakking, and A. Rouzée, "Evolution of a molecular shape resonance along a stretching chemical bond," Phys. Rev. Lett. **125**, 123001 (2020).
25. C. D. Lin, A.-T. Le, Z. Chen, T. Morishita, and R. Lucchese, "Strong-field rescattering physics—self-imaging of a molecule by its own electrons," J. Phys. B **43**, 122001 (2010).
26. L. Brugnera, D. J. Hoffmann, T. Siegel, F. Frank, A. Zaïr, J. W. G. Tisch, and J. P. Marangos, "Trajectory selection in high harmonic generation by controlling the phase between orthogonal two-color fields," Phys. Rev. Lett. **107**, 153902 (2011).
27. M. Lewenstein, P. Balcou, M. Y. Ivanov, A. L'Huillier, and P. B. Corkum, "Theory of high-harmonic generation by low-frequency laser fields," Phys. Rev. A **49**, 2117–2132 (1994).
28. E. Takahashi, Y. Nabekawa, and K. Midorikawa, "Generation of 10-μj coherent extreme-ultraviolet light by use of high-order harmonics," Opt. Lett. **27**, 1920–1922 (2002).
29. S. Hädrich, J. Rothhardt, M. Krebs, S. Demmler, A. Klenke, A. Tünnermann, and J. Limpert, "Single-pass high harmonic generation at high repetition rate and photon flux," J. Phys. B **49**, 172002 (2016).
30. I. Makos, I. Orfanos, A. Nayak, J. Peschel, B. Major, I. Liontos, E. Skantzakis, N. Papadakis, C. Kalpouzos, M. Dumergue, S. Kühn, K. Varju, P. Johnsson, A. L'Hullier, P. Tzallas, and D. Charalambidis, "A 10-gigawatt attosecond source for non-linear XUV optics and XUV-pump-XUV-probe studies," Sci. Rep. **10**, 3759 (2020).

31. H.-W. Sun, P.-C. Huang, Y.-H. Tzeng, J.-T. Huang, C. D. Lin, C. Jin, and M.-C. Chen, "Extended phase matching of high harmonic generation by plasma-induced defocusing," Optica **4**, 976–981 (2017).
32. Y. Tamaki, J. Itatani, Y. Nagata, M. Obara, and K. Midorikawa, "Highly efficient, phase-matched high-harmonic generation by a self-guided laser beam," Phys. Rev. Lett. **82**, 1422 (1999).
33. J. R. Sutherland, E. L. Christensen, N. D. Powers, S. E. Rhynard, J. C. Painter, and J. Peatross, "High harmonic generation in a semi-infinite gas cell," Opt. Express **12**, 4430–4436 (2004).
34. P. Rudawski, C. M. Heyl, F. Brizuela, J. Schwenke, A. Persson, E. Mansten, R. Rakowski, L. Rading, F. Campi, B. Kim, P. Johnsson, and A. L'Huillier, "A high-flux high-order harmonic source," Rev. Sci. Instrum. **84**, 073103 (2013).
35. A. Rundquist, C. G. Durfee, Z. Chang, C. Herne, S. Backus, M. M. Murnane, and H. C. Kapteyn, "Phase-matched generation of coherent soft x-rays," Science **280**, 1412–1415 (1998).
36. T. Pfeifer, R. Kemmer, R. Spitzenpfeil, D. Walter, C. Winterfeldt, G. Gerber, and C. Spielmann, "Spatial control of high-harmonic generation in hollow fibers," Opt. Lett. **30**, 1497–1499 (2005).
37. A. Paul, E. Gibson, X. Zhang, A. Lytle, T. Popmintchev, X. Zhou, M. Murnane, I. Christov, and H. Kapteyn, "Phase-matching techniques for coherent soft x-ray generation," IEEE J. Quantum Electron. **42**, 14–26 (2006).
38. T. Popmintchev, M.-C. Chen, A. Bahabad, M. Gerrity, P. Sidorenko, O. Cohen, I. P. Christov, M. M. Murnane, and H. C. Kapteyn, "Phase matching of high harmonic generation in the soft and hard x-ray regions of the spectrum," Proc. Natl. Acad. Sci. USA **106**, 10516 (2009).
39. P. Balcou, P. Saliéres, A. L'Huillier, and M. Lewenstein, "Generalized phase-matching conditions for high harmonics: the role of field-gradient forces," Phys. Rev. A **55**, 3204 (1997).
40. L. Hareli, G. Shoulga, and A. Bahabad, "Phase matching and quasi-phase matching of high-order harmonic generation—a tutorial," J. Phys. B **53**, 233001 (2020).
41. S. Adachi, T. Horio, and T. Suzuki, "Generation of intense single-order harmonic pulse in the vacuum ultraviolet region using a deep ultraviolet driving laser," Opt. Lett. **37**, 2118–2120 (2012).
42. D. Popmintchev, C. Hernández-García, F. Dollar, C. Mancuso, J. A. Pérez-Hernández, M.-C. Chen, A. Hankla, X. Gao, B. Shim, A. L. Gaeta, M. Tarazkar, D. A. Romanov, R. J. Levis, J. A. Gaffney, M. Foord, S. B. Libby, A. Jaron-Becker, A. Becker, L. Plaja, M. M. Murnane, H. C. Kapteyn, and T. Popmintchev, "Ultraviolet surprise: efficient soft x-ray high-harmonic generation in multiply ionized plasmas," Science **350**, 1225 (2015).
43. H. Wang, Y. Xu, S. Ulonska, J. S. Robinson, P. Ranitovic, and R. A. Kaindl, "Bright high-repetition-rate source of narrowband extreme-ultraviolet harmonics beyond 22 eV," Nat. Commun. **6**, 7459 (2015).
44. C. Marceau, T. J. Hammond, A. Y. Naumov, P. B. Corkum, and D. M. Villeneuve, "Wavelength scaling of high harmonic generation for 267 nm, 400 nm and 800 nm driving laser pulses," J. Phys. Commun. **1**, 015009 (2017).
45. S. Adachi and T. Suzuki, "UV-driven harmonic generation for time-resolved photoelectron spectroscopy of polyatomic molecules," Appl. Sci. **8**, 1784 (2018).
46. S. Watanabe, K. Kondo, Y. Nabekawa, A. Sagisaka, and Y. Kobayashi, "Two-color phase control in tunneling ionization and harmonic generation by a strong laser field and its third harmonic," Phys. Rev. Lett. **73**, 2692 (1994).
47. U. Andiel, G. D. Tsakiris, E. Cormier, and K. Witte, "High-order harmonic amplitude modulation in two-colour phase-controlled frequency mixing," Europhys. Lett. **47**, 42 (1999).
48. E. Cormier and M. Lewenstein, "Optimizing the efficiency in high order harmonic generation optimization by two-color fields," Eur. Phys. J. D **12**, 227 (2000).
49. I. Kim, C. Kim, H. Kim, G. Lee, Y. Lee, J. Park, D. Cho, and C. Nam, "Highly efficient high-harmonic generation in an orthogonally polarized two-color laser field," Phys. Rev. Lett. **94**, 243901 (2005).
50. L. E. Chipperfield, J. S. Robinson, J. W. G. Tisch, and J. P. Marangos, "Ideal waveform to generate the maximum possible electron recollision energy for any given oscillation period," Phys. Rev. Lett. **102**, 063003 (2009).
51. G. Lambert, J. Gautier, C. P. Hauri, P. Zeitoun, C. Valentin, T. Marchenko, F. Tissandier, J. P. Goddet, M. Ribiere, G. Rey, M. Fajardo, and S. Sebban, "An optimized kHz two-colour high harmonic source for seeding free-electron lasers and plasma-based soft x-ray lasers," New J. Phys. **11**, 083033 (2009).
52. L. Brugnera, F. Frank, D. J. Hoffmann, R. Torres, T. Siegel, J. G. Underwood, E. Springate, C. Froud, E. I. C. Turcu, J. W. G. Tisch, and J. P. Marangos, "Enhancement of high harmonics generated by field steering of electrons in a two-color orthogonally polarized laser field," Opt. Lett. **35**, 3994–3996 (2010).
53. O. Raz, O. Pedatzur, B. D. Bruner, and N. Dudovich, "Spectral caustics in attosecond science," Nat. Photonics **6**, 170–173 (2012).
54. J. A. Pérez-Hernández, M. F. Ciappina, M. Lewenstein, L. Roso, and A. Zar, "Beyond carbon k-edge harmonic emission using a spatial and temporal synthesized laser field," Phys. Rev. Lett. **110**, 053001 (2013).
55. P. Wei, J. Miao, Z. Zeng, C. Li, X. Ge, R. Li, and Z. Xu, "Selective enhancement of a single harmonic emission in a driving laser field with subcycle waveform control," Phys. Rev. Lett. **110**, 233903 (2013).
56. F. Brizuela, C. M. Heyl, P. Rudawski, D. Kroon, L. Rading, J. M. Dahlström, J. Mauritsson, P. Johnsson, C. L. Arnold, and A. L'Huillier, "Efficient high-order harmonic generation boosted by below-threshold harmonics," Sci. Rep. **3**, 1410 (2013).
57. P. Wei, Z. Zeng, J. Jiang, J. Miao, Y. Zheng, X. Ge, C. Li, and R. Li, "Selective generation of an intense single harmonic from a long gas cell with loosely focusing optics based on a three-color laser field," Appl. Phys. Lett. **104**, 151101 (2014).
58. C. Jin, G. Wang, H. Wei, A.-T. Le, and C. D. Lin, "Waveforms for optimal sub-keV high-order harmonics with synthesized two- or three-colour laser fields," Nat. Commun. **5**, 4003 (2014).
59. S. Haessler, T. Balčiunas, G. Fan, G. Andriukaitis, A. Pugžlys, A. Baltuška, T. Witting, R. Squibb, A. Zaïr, J. W. G. Tisch, J. P. Marangos, and L. E. Chipperfield, "Optimization of quantum trajectories driven by strong-field waveforms," Phys. Rev. X **4**, 021028 (2014).
60. T. Kroh, C. Jin, P. Krogen, P. D. Keathley, A.-L. Calendron, J. P. Siqueira, H. Liang, E. L. Falcão-Filho, C. D. Lin, F. X. Kärtner, and K.-H. Hong, "Enhanced high-harmonic generation up to the soft x-ray region driven by mid-infrared pulses mixed with their third harmonic," Opt. Express **26**, 16955–16969 (2018).
61. M. Sayrac, A. A. Kolomenskii, J. Dong, and H. A. Schuessler, "Generation of enhanced even harmonics of fundamental radiation in temporally separated two-color laser fields," J. Electron Spectros. Relat. Phenom. **233**, 22 (2019).
62. S. Mitra, S. Biswas, J. Schötz, E. Pisanty, B. Förg, G. A. Kavuri, C. Burger, W. Okell, M. Hügner, I. Pupeza, V. Pervak, M. Lewenstein, P. Wnuk, and M. F. Kling, "Suppression of individual peaks in two-colour high harmonic generation," J. Phys. B **53**, 134004 (2020).
63. A. Zaïr, M. Holler, A. Guandalini, F. Schapper, J. Biegert, L. Gallmann, U. Keller, A. S. Wyatt, A. Monmayrant, I. A. Walmsley, E. Cormier, T. Auguste, J. P. Caumes, and P. Salières, "Quantum path interferences in high-order harmonic generation," Phys. Rev. Lett. **100**, 143902 (2008).
64. S. R. Abbing, F. Campi, F. S. Sajjadian, N. Lin, P. Smorenburg, and P. M. Kraus, "Divergence control of high-harmonic generation," Phys. Rev. Appl. **13**, 054029 (2020).
65. X. Ren, V. Makhija, A.-T. Le, J. Troß, S. Mondal, C. Jin, V. Kumarappan, and C. Trallero-Herrero, "Measuring the angle-dependent photoionization cross section of nitrogen using high-harmonic generation," Phys. Rev. A **88**, 043421 (2013).
66. B. Langdon, J. Garlick, X. Ren, D. J. Wilson, A. M. Summers, S. Zigo, M. F. Kling, S. Lei, C. G. Elles, E. Wells, E. D. Poliakoff, K. D. Carnes, V. Kumarappan, I. Ben-Itzhak, and C. A. Trallero-Herrero, "Carrier-envelope-phase stabilized terawatt class laser at 1 kHz with a wavelength tunable option," Opt. Express **23**, 4563–4572 (2015).
67. C. Burger, W. F. Frisch, T. M. Kardas, M. Trubetskov, V. Pervak, R. Moshammer, B. Bergues, M. F. Kling, and P. Wnuk, "Compact and flexible harmonic generator and three-color synthesizer for femtosecond coherent control and time-resolved studies," Opt. Express **25**, 31130–31139 (2017).
68. T. Kita, T. Harada, N. Nakano, and H. Kuroda, "Mechanically ruled aberration-corrected concave gratings for a flat-field grazing-incidence spectrograph," Appl. Opt. **22**, 512–513 (1983).
69. A. Kramida, Y. Ralchenko, and J. Reader, and NIST ASD Team, "NIST atomic spectra database (ver. 5.8)," National Institute of Standards and Technology, 2020, https://physics.nist.gov/asd.
70. W.-H. Xiong, L.-Y. Peng, and Q. Gong, "Recent progress of below-threshold harmonic generation," J. Phys. B **50**, 032001 (2017).

71. N. Ishii, A. Kosuge, T. Hayashi, T. Kanai, J. Itatani, S. Adachi, and S. Watanabe, "Quantum path selection in high-harmonic generation by a phase-locked two-color field," Opt. Express **16**, 20876–20883 (2008).
72. M. B. Gaarde, J. L. Tate, and K. J. Schafer, "Macroscopic aspects of attosecond pulse generation," J. Phys. B **41**, 132001 (2008).
73. C. Trallero-Herrero, C. Jin, B. E. Schmidt, A. D. Shiner, J.-C. Kieffer, P. B. Corkum, D. M. Villeneuve, C. D. Lin, F. Légaré, and A.-T. Le, "Generation of broad XUV continuous high harmonic spectra and isolated attosecond pulses with intense mid-infrared lasers," J. Phys. B **45**, 011001 (2011).
74. A. D. Shiner, C. Trallero-Herrero, N. Kajumba, H.-C. Bandulet, D. Comtois, F. Légaré, M. Giguère, J.-C. Kieffer, P. B. Corkum, and D. M. Villeneuve, "Wavelength scaling of high harmonic generation efficiency," Phys. Rev. Lett. **103**, 073902 (2009).
75. A. Shiner, C. Trallero-Herrero, N. Kajumba, B. Schmidt, J. Bertrand, K. T. Kim, H.-C. Bandulet, D. Comtois, J.-C. Kieffer, D. Rayner, P. Corkum, F. Légaré, and D. Villeneuve, "High harmonic cutoff energy scaling and laser intensity measurement with a 1.8 m laser source," J. Mod. Opt. **60**, 1458 (2013).
76. P. B. Corkum, "Plasma perspective on strong field multiphoton ionization," Phys. Rev. Lett. **71**, 1994 (1993).
77. J. L. Krause, K. J. Schafer, and K. C. Kulander, "High-order harmonic generation from atoms and ions in the high intensity regime," Phys. Rev. Lett. **68**, 3535 (1992).
78. M. B. Gaarde, F. Salin, E. Constant, P. Balcou, K. J. Schafer, K. C. Kulander, and A. L'Huillier, "Spatiotemporal separation of high harmonic radiation into two quantum path components," Phys. Rev. A **59**, 1367 (1999).
79. F. Schapper, M. Holler, T. Auguste, A. Zaïr, M. Weger, P. Salières, L. Gallmann, and U. Keller, "Spatial fingerprint of quantum path interferences in high order harmonic generation," Opt. Express **18**, 2987–2994 (2010).
80. X. He, J. M. Dahlström, R. Rakowski, C. M. Heyl, A. Persson, J. Mauritsson, and A. L'Huillier, "Interference effects in two-color high-order harmonic generation," Phys. Rev. A **82**, 033410 (2010).
81. H. Wikmark, C. Guo, J. Vogelsang, P. W. Smorenburg, H. Coudert-Alteirac, J. Lahl, J. Peschel, P. Rudawski, H. Dacasa, S. Carlström, S. Maclot, M. B. Gaarde, P. Johnsson, C. L. Arnold, and A. L'Huillier, "Spatiotemporal coupling of attosecond pulses," Proc. Natl. Acad. Sci. USA **116**, 4779–4784 (2019).
82. L. Quintard, V. Strelkov, J. Vabek, O. Hort, A. Dubrouil, D. Descamps, F. Burgy, C. Péjot, E. Mével, F. Catoire, and E. Constant, "Optics-less focusing of XUV high-order harmonics," Sci. Adv. **5**, eaau7175 (2019).